# Assessment of Complex Radiated EMC Problems Involving Slotted Enclosures Using a 2-D Generalized Circuital Approach

Juan V. Balbastre, Luis Nuño, *Member, IEEE*, Alejandro Díaz-Morcillo, *Member, IEEE*, and Antonio Lozano

***Abstract*—A 2-D version of the generalized circuital analysis (GCA) has been used along with the finite element method (FEM) to estimate both the radiated perturbation produced by an arbitrary current distribution (represented by a set of linear current sources) covered by a slotted enclosure, and the field coupled to a slotted screen due to a radiated perturbation. The effect of a given enclosure is modeled by means of a scattering matrix (which depends only on its geometry) obtained by the FEM. On the other hand, any arbitrary perturbating field can be expanded in a series of cylindrical harmonics, and then, the total field is computed everywhere using the scattering matrices. This method has the advantage over conventional FEM approaches that FEM is applied only once, and then a wide range of electromagnetic compatibility (EMC) problems can be solved with almost no extra computational effort. Two-dimensional models of relevant EMC problems involving both emission and immunity have been studied in order to extract useful information for actual 3-D systems. In spite of the 2-D approach, very interesting conclusions can be derived from the examples presented in this paper (like the effect of slot resonances in the field distribution within slotted enclosures or the coupling between two connected cavities).**

***Index Terms*—Electromagnetic compatibility (EMC), generalized circuital analysis (GCA), intrasystem problems, radiated emissions and susceptibility.**

## I. Introduction

ELECTRONIC circuits are often covered by some kind of screen or enclosure in order to avoid their radiation and to protect them from external electromagnetic interferences. However, these enclosures are usually slotted in order to allow the connection of the covered circuit to the exterior world (the expansion slots in personal computers (PCs) are a very common example). Thus, electromagnetic fields radiated by some apparatus can penetrate inside the enclosure of another devices and affect their correct performance (intersystem perturbations). Hence, the knowledge of the radiation characteristics and the coupling properties of slotted enclosures, which depend on frequency and polarization, can help to improve circuit design. On the other hand, there are electronic subsystems being part of more complex electronic systems. In this case, electromagnetic interferences coming from one part of the system can affect the normal operation of the whole system itself (intrasystem perturbation). In this case, the task of the design engineer, from the point of view of electromagnetic compatibility (EMC), deals with finding the best layout so that the spurious coupling between different parts of the system is kept as low as possible.

The analytical solution of EMC problems is seldom possible, since it involves the solution of Maxwell's equations in inhomogeneous, arbitrarily shaped, and often open regions; thus, they must be numerically solved. Indeed, nowadays there are many commercial packages based on different numerical methods readily available for being used in EMC-oriented design. However, EMC problems are really so complex that even when they are solved using well-established numerical methods, like the finite-difference time-domain method (FDTD) or the finite element method (FEM), the numerical models used for the analysis must be thoroughly designed and their results carefully considered. In the last few years, several studies of EMC problems related with slotted enclosures have been published ([1]–[3] are representative samples), most of them dealing with the computation of the shielding effectiveness (SE) at some fixed positions inside the enclosure, or the radiated perturbations produced by a coaxial probe somewhere within the shield.

In this paper, a hybrid method consisting of a combination of FEM and modal analysis (MA), the so-called generalized circuital analysis (GCA) [4] is used to study the 2-D slotted enclosures of arbitrary geometry and composition, from the point of view of EMC. The 2-D approach has been used in order to reduce the complexity of the analysis, and to make it possible to obtain estimates of the actual electromagnetic perturbations in a reasonable time using single-processor computers. The GCA method allows to characterize a given enclosure independently of the perturbation field, so that any emission or immunity problem involving that shield can be studied without solving a FEM problem for each particular excitation. Although the results obtained are quantitatively approximate, they are qualitatively meaningful, and provide a very interesting insight into what is actually happening within the enclosure. The results presented in this work can be used both by engineers dealing with EMC problems to assess design guidelines and by researchers to help them to define further 3-D models for future research works.

In Section II, the fundamentals of the GCA are briefly outlined (for a deeper description, see [4]), and the circuital models for both radiated intersystem and intrasystem EMC problems are derived. For the sake of concision, only $TM^z$ polarized waves are considered herein, being very similar to the analysis of $TE^z$ waves [4]. In Section III, the proposed method is validated by

Manuscript received July 13, 2005; revised April 13, 2007.

J. V. Balbastre and L. Nuño are with the ITACA Research Institute, Polytechnic University of Valencia, Valencia 46022, Spain (e-mail: jbalbast@itaca.upv.es; lnuno@itaca.upv.es).

A. Díaz-Morcillo and A. Lozano are with the Department of Information Technologies and Communications, Polytechnic University of Cartagena (UPCT), Cartagena 30202, Spain (e-mail: Alejandro.Morcillo@upct.es; Antonio.Lozano@upct.es).

Color versions of one or more of the figures in this paper are available online at http://ieeexplore.ieee.org.

Digital Object Identifier 10.1109/TEMC.2007.902400

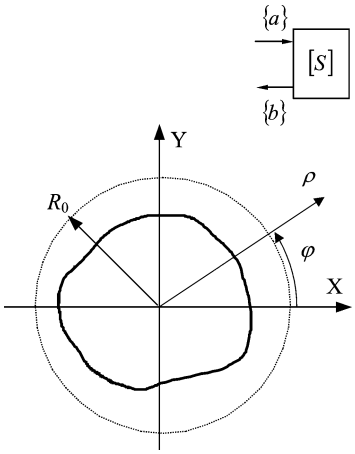


Fig. 1. General representation of a one-port network and the equivalent circuital model.

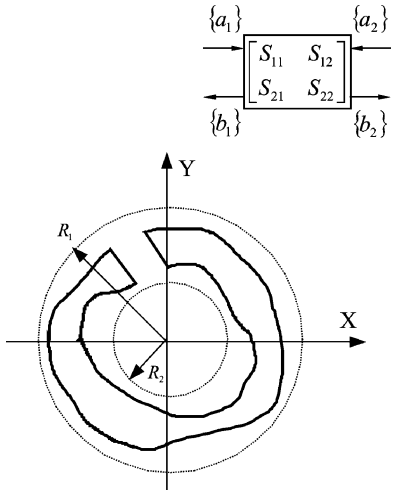


Fig. 2. General representation of a two-port network and the equivalent circuital model.

comparing simulated results and measurements, and then several numerical examples are solved in order to show how a 2-D simulation tool provides useful qualitative results when properly applied to relevant EMC problems. The conclusions of this work are presented in Section IV. Time-harmonic electromagnetic fields with $e^{j\omega t}$ time variation are used throughout this paper, and they are represented by their complex amplitude or phasor.

## II. Theory

### A. Circuital Characterization of One-Port Networks

The more general one-port network is formed by a 2-D region contained in the *XY* plane and enclosed within a circumference of radius $R_0$, as can be seen in Fig. 1. This circumference is called access or port, using the microwave network analysis terminology. At the port, the incoming (represented by the superscript $+$) and outgoing (represented by the superscript $-$) electric field wave amplitudes can be expanded as [5]

$$E_z^+ = \sum_{n=-N}^{N} a_n H_n^{(1)}(k_0 R_0)\, e^{jn\phi} \tag{1a}$$

$$E_z^- = \sum_{n=-N}^{N} b_n H_n^{(2)}(k_0 R_0)\, e^{jn\phi} \tag{1b}$$

where $k_0 = \omega\sqrt{\mu_0 \varepsilon_0}$ is the free-space wavenumber, $H_n^{(1)}(x)$ and $H_n^{(2)}(x)$ are the Hankel functions of the first and second kind and order $n$, respectively, and the modal coefficients $a_n$ and $b_n$ are the elements of vectors $\{a\}$ and $\{b\}$ defined in Fig. 1. The number of terms used in the modal expansion is $N \cong k_0 R_0$, so that the electric field can be properly obtained in the region $\rho \geq R_0$ [6], [7].

The modal coefficient vectors are related by means of a generalized scattering matrix $[S]$ as

$$\{b\} = [S]\{a\}. \tag{2}$$

The generalized admittance matrix (GAM) relating the total electric and magnetic fields tangential to the circumference defining the access is the basis for the computation of the generalized scattering matrix. The first step to construct the GAM matrix is to compute the magnetic field $H_{\phi,n}|_{\rho=R_0}$ using the FEM with the boundary condition $E_{z,n}|_{\rho=R_0} = e^{jn\phi}$ for $-N \leq n \leq N$.

The admittance parameters are then defined as

$$H_{\phi,n}|_{\rho=R_0} = \sum_{m=-N}^{N} Y_{m,n} e^{jm\phi} \tag{3}$$

and they are computed by using the orthogonality property of complex exponentials as

$$Y_{m,n} = \frac{1}{2\pi}\int_0^{2\pi} H_{\phi,n}|_{\rho=R_0} e^{-jm\phi} d\phi, \qquad -N \leq m,n \leq N. \tag{4}$$

Finally, enforcing the continuity of both the total tangential electric and magnetic fields, the scattering matrix of (2) is obtained [4].

### B. Circuital Characterization of Two-Port Networks

A two-port network is considered to be formed by a 2-D region lying on the *XY* plane, and bounded by two circumferences of radii $R_1$ and $R_2$, as shown in Fig. 2. The circumference of radius $R_1$ is also called port $n^\circ$ 1, and that of radius $R_2$, port $n^\circ$ 2. At both ports, the incoming and outgoing waves can be expanded in terms of cylindrical harmonics, as in the case of one-port networks. The number of modes used in these expansions is $N_1 \cong k_0 R_1$ at port $n^\circ$ 1 and $N_2 \cong k_0 R_2$ at port $n^\circ$ 2, in order to properly represent the electric fields at $\rho \geq R_1$ and $\rho = R_2$ [6], [7]. The modal coefficient vectors $\{a_1\}, \{b_1\}, \{a_2\}$, and $\{b_2\}$ are defined in Fig. 2, and they are related by means of a generalized scattering matrix

$$\begin{Bmatrix} \{b_1\} \\ \{b_2\} \end{Bmatrix} = \begin{bmatrix} [S_{11}] & [S_{12}] \\ [S_{21}] & [S_{22}] \end{bmatrix} \begin{Bmatrix} \{a_1\} \\ \{a_2\} \end{Bmatrix}. \tag{5}$$

This scattering matrix is derived from a GAM, as in the one-port case described in Section II-A. The two-port GAM is also

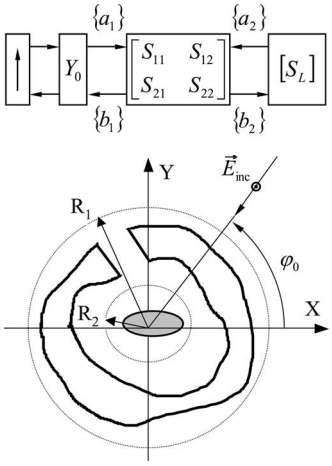


Fig. 3. Definition of the general radiated susceptibility problem.

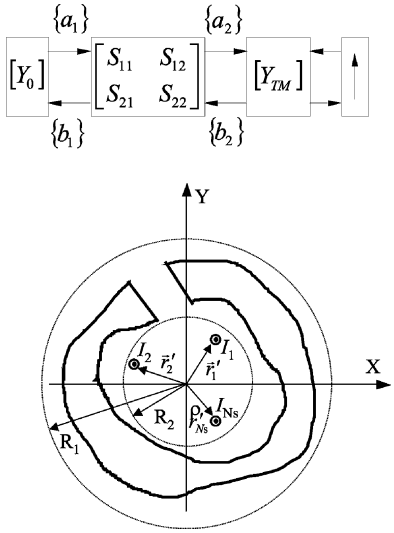


Fig. 4. General radiated emission problem. Several linear current sources are arbitrarily distributed inside a slotted envelope.

computed following a very similar procedure than that used in the one-port case [4].

### C. Spectral Representation of Perturbating Fields

Two perturbation sources are considered in the EMC problems dealt with in this paper: plane wave incidence (radiated susceptibility) and arbitrary currents (radiated emission and intrasystem problems). The plain wave decomposition into cylindrical harmonics is given by [5]

$$E_z = \sum_{n=-\infty}^{\infty} E_0\, e^{-jn\left(\frac{\pi}{2}+\varphi_0\right)}\, J_n(k_0\rho)\, e^{jn\varphi} \tag{6}$$

where $E_0$ is the electric field perturbations amplitude, $J_n(x)$ is the Bessel function of the first kind and order $n$, and $\varphi = \varphi_0$ is the angle of incidence, as defined in Fig. 3.

On the other side, arbitrary currents are approximated by a set of linear current sources. The electric field produced at an arbitrary point $\vec{r}$ by a linear current source centered at point $\vec{r}\,'$ of cylindrical coordinates $(\rho', \varphi')$ and radiating in the free-space is given by

$$E_z(\vec{r}) = -30\pi k_0 I_0 H_0^{(2)}(k_0|\vec{r} - \vec{r}\,'|) \tag{7}$$

where $I_0$ is the current amplitude. Using the addition theorem of Hankel functions, it is possible to expand the perturbating field at point $\vec{r}$ in terms of centered cylindrical harmonics [8]

$$E_z(\vec{r}) = -30 k_0 I_0 \times \begin{cases} \sum_{n=-\infty}^{\infty} H_n^{(2)}(k_0\rho')\, J_n(k_0\rho)\, e^{jn(\varphi-\varphi')} & \rho \le \rho' \\ \sum_{n=-\infty}^{\infty} J_n(k_0\rho')\, H_n^{(2)}(k_0\rho)\, e^{jn(\varphi-\varphi')} & \rho \ge \rho'. \end{cases} \tag{8}$$

### D. Circuital Analysis of Radiated Susceptibility

If the perturbation source is far away from the victim system, the perturbating electric field can be locally represented by a plane wave. Fig. 3 shows the general geometry and the equivalent circuit for this case. Taking into account the definition of the Hankel functions of the first and second kind [8] and the modal expansion of a plane wave in terms of cylindrical harmonics (6) the $a_{1n}$ coefficients are given by

$$a_{1n} = \frac{E_0}{2} e^{-jn\left(\frac{\pi}{2}+\varphi_0\right)}. \tag{9}$$

This perturbation is included in the equivalent circuit of Fig. 3 as a matched current source, since the fields scattered by the enclosure are not reflected back toward the origin (Sommerfeld condition at $\rho \to \infty$). On the other hand, the victim cylinder is represented by a one-port network scattering matrix $[S_L]$, used to load the port $n^\circ$ 2 in the equivalent transmission line model represented in Fig. 3. In this work, the radiated susceptibility analysis has been focused on empty enclosures. In this particular case, since there is nothing within the enclosure neither absorbing nor reflecting incoming energy, $\{a_2\} = \{b_2\}$, i.e., the load scattering matrix in the equivalent circuit of Fig. 3 is the identity matrix. For the case of empty enclosures, the modal coefficient vectors are, hence, given by

$$\{b_1\} = [S_{11}]\{a_1\} + [S_{12}]\,[[I] - [S_{22}]]\,[S_{21}]\,\{a_1\} \tag{10a}$$

$$\{a_2\} = \{b_2\} = [[I] - [S_{22}]]^{-1}\,[S_{21}]\,\{a_1\}. \tag{10b}$$

Even in this simple case, the electrical field within the enclosure must be computed using numerical methods. A FEM solution can be easily obtained once the total electric field at $\rho = R_1$ and $\rho = R_2$ has been computed [9].

### E. Circuital Analysis of Radiated Emissions

The general case of radiated emissions considered in this work is represented in Fig. 4, along with its circuital model. The arbitrary perturbating current, represented by a set of $N_S$ linear current sources of amplitude $I_i$ and placed at $(\rho_i', \varphi_i')$, is included in the circuital model as a matched current source. Assuming that $R_2 \ge \max\{\rho_i'\}$ and from (8), the modal coefficients of the

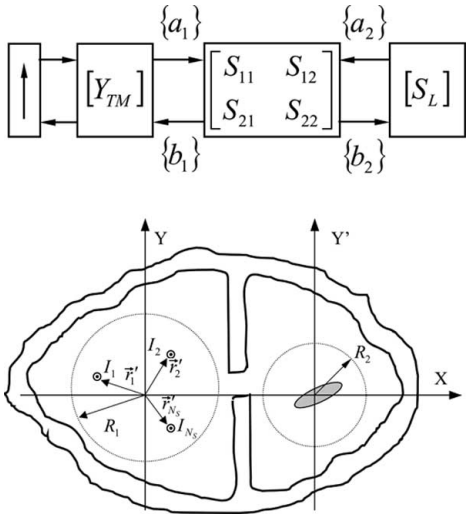


Fig. 5. General intrasystem EMC problem with an arbitrary set of linear current sources inducing perturbating fields in other shielded parts of the circuit.

incoming waves at port $n^\circ$ 2 are given by

$$a_{2n} = -30\pi k_0 \sum_{i=1}^{N_S} I_i \, J_n(k_0\rho_i') \, e^{-jn\varphi_i'}. \tag{11}$$

On the other side, since the Sommerfeld condition at $\rho \to \infty$ states that $a_{1n} = 0$ (there is no reflection from the "surface at infinity"), port $n^\circ$ 2 is loaded with the free-space admittance in the circuital model of Fig. 4. Finally, the arbitrarily shaped slotted screen enclosing the currents is represented by a two-port scattering matrix. Thus, from (5) we have

$$\{b_1\} = [S_{12}]\,\{a_2\} \tag{12a}$$

$$\{b_2\} = [S_{22}]\,\{a_2\}. \tag{12b}$$

If the victim circuit is outside the enclosure, the electric field perturbation radiated by the shielded current is given by

$$E_z = \sum_{n=-N_1}^{N_1} b_{1n} H_n^{(2)}(k_0\rho)\, e^{jn\phi} \qquad \rho \geq R_1 \tag{13}$$

since the region $\rho \geq R_1$ is assumed to be homogeneous, and the number of modes used in the circuital analysis ($N_1 \cong k_0 R_1$) is big enough to guarantee that (13) converges to the actual field.

If the victim system is far away, (13) can be simplified using the asymptotic form of the Hankel functions of the second order for big arguments [8] as

$$E_z = \sqrt{\frac{2j}{\pi k_0 \rho}} e^{-jk_0\rho} \sum_{n=-N_1}^{N_1} b_{1n} e^{jn\left(\phi+\frac{\pi}{2}\right)}, \qquad k_0\rho \gg 1. \tag{14}$$

### F. Circuital Analysis of Intrasystem EMC Problems

Fig. 5 represents the general geometry used in this paper to represent an EMC intrasystem problem and the corresponding equivalent circuit. The cavity on the left contains the more noisy elements of the circuit, represented by a set of linear current sources (a matched current source in the equivalent circuit). The cavity on the right holds the more electromagnetically susceptible elements of the circuit, represented by an arbitrarily shaped cylinder included in the circuital model as a one-port scattering matrix loading the port $n^\circ$ 2. The modal coefficients representing the current perturbation in the transmission line model of Fig. 5 are

$$a_{1n} = -30\pi k_0 \sum_{i=1}^{N_S} I_i J_n(k_0\rho_i')\, e^{-jn\varphi_i'}. \tag{15}$$

If the scattering matrix representing the victim cylinder is $[S_L]$, the unknown coefficients can be identified as

$$\{b_1\} = [S_{11}]\,\{a_1\} + [S_{12}]\,[S_L]\,\left[[I] - [S_{22}]\,[S_L]\right]^{-1}\,[S_{21}]\,\{a_1\} \tag{16a}$$

$$\{a_2\} = [S_L]\,\left[[I] - [S_{22}]\,[S_L]\right]^{-1}[S_{21}]\,\{a_1\} \tag{16b}$$

$$\{b_2\} = \left[[I] - [S_{22}]\,[S_L]\right]^{-1}[S_{21}]\,\{a_1\}. \tag{16c}$$

The particular case of a perfectly conducting centered cylinder of radius $R$ is considered in the following section. In this case, the one-port scattering matrix can be easily derived using the MA technique [5], and it is given by

$$[S_L]_{n,n} = -\frac{H_n^{(1)}(k_0R)}{H_n^{(2)}(k_0R)}, \qquad -N_2 \leq n \leq N_2. \tag{17}$$

Finally, the total electric field within the enclosure is numerically computed as in the radiated susceptibility case described in Sections II–IV.

## III. Numerical Examples

In this section, the proposed method is validated by computing the SE of a rectangular enclosure with the size of a typical main unit of a PC with a slot having the dimensions of a CD-ROM reader, which is a widely referred example. Then, three examples of the most outstanding EMC problems are presented in this section, covering both the radiated and intrasystem cases. The first example deals with the emission problem. A squared slotted enclosure is analyzed in order to explore the relation between the SE and the slot length. The effect of the unshielded electric field perturbation pattern is also considered. In the second example, one system formed by two connected identical squared cavities is studied, considering the victim cavity either empty and containing a conducting cylinder. Both common mode and differential mode perturbations are considered. Finally, a radiated susceptibility problem has been solved to show the effect of finite electrical losses on the shield performance.

### A. Validation

To validate the proposed 2-D method, the SE of the empty enclosure of Fig. 6 was computed. The SE is defined as [10]

$$\text{SE(dB)} = -20\log\left(\frac{|\vec{E}_0|}{|\vec{E}_S|}\right) \tag{18}$$

where $\vec{E}_S$ is the electric field somewhere within the enclosure and $\vec{E}_0$ is the electric field present at the same point when the

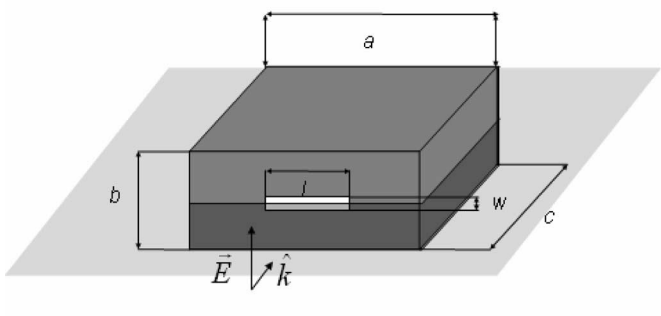


Fig. 6. Geometry of the slotted rectangular box used to validate the 2-D approach ($a = 30$ cm, $b = 12$ cm, $c = 30$ cm, $l = 10$ cm, and $w = 0.5$ cm). The plane represents the cut where the 2-D computation is carried out.

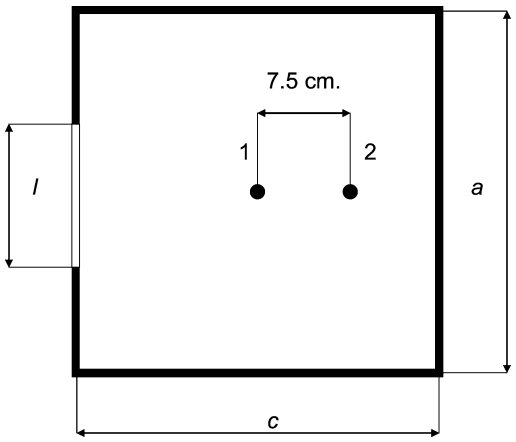


Fig. 7. Position of the probes used to measure the field inside the enclosure and where the SE is computed.

shield is removed. In this example, $\vec{E}_0$ is a plane wave linearly polarized in a direction orthogonal to the slot, as shown in Fig. 6, and $\vec{E}_S$ was computed between 100 MHz and 2 GHz using a 2-D model of the structure in two locations within the enclosure (see Fig. 7). Then, the 3-D SE can be obtained by using the expression [11]

$$\mathrm{SE(dB)} = \mathrm{SE_{2D}(dB)} + 10\log_{10}\left(\frac{b}{w}\right). \tag{19}$$

The simulated SE is plotted in Figs. 8 and 9, along with the corresponding measurements showing a very good agreement. Regarding the computational effort, the SE was computed at 1000 frequency points in 20 min on a 2.66-GHz Pentium IV by means of the 2-D approach using a FEM mesh of less than 1000 elements. Similar results can be obtained using a 3-D solver (ANSYS). The model had more than 50 000 unknowns, and the problem was solved in 650 min of CPU time on a COMPAQ DS20 single-processor computer (and using only 400 frequency points).

### *B. Radiated Emission*

Fig. 10 shows a square enclosure of side $W$ with a slot of length $a = 0.2W$ on the top, containing a 1-A linear electric current source along the Z-axis. The normalized electric

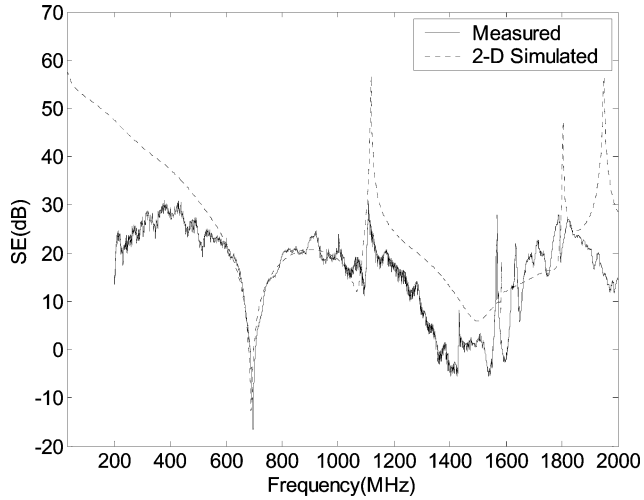


Fig. 8. Comparison between the SE computed using the 2-D approach and that measured at position 1 (see Fig. 9).

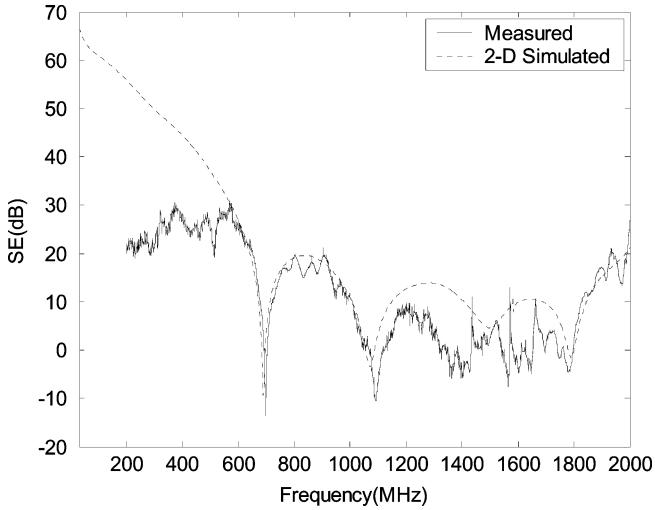


Fig. 9. Comparison between the SE computed using the 2-D approach and that measured at position 2.

field perturbation radiated along the positive Y-axis direction is plotted versus the free-space wavenumber. As expected from the slot antenna theory (see [12]), the maximum radiation is achieved for the resonant slot ($a = \lambda/2,\ k_0 = 4\pi/a$). Fig. 10 also shows the electric field pattern within the enclosure for resonant and nonresonant enclosures. Special attention must be paid to the strong modification of the electric field pattern within the enclosure due to the slot resonance, since the perturbation field can be up to 10 dB higher than the corresponding nonresonant values near the conducting walls.

In order to explore the effect of the unshielded perturbation pattern on the perturbation strength, the same square slotted enclosure has been analyzed, but now enclosing two linear current sources. The amplitude of all the interfering current sources is 1 A, but different phases, separations, and emplacements have been considered. The unshielded radiated electric field patterns are shown in Fig. 11, along with the electric field perturbations radiated by the shielded currents around the enclosure through

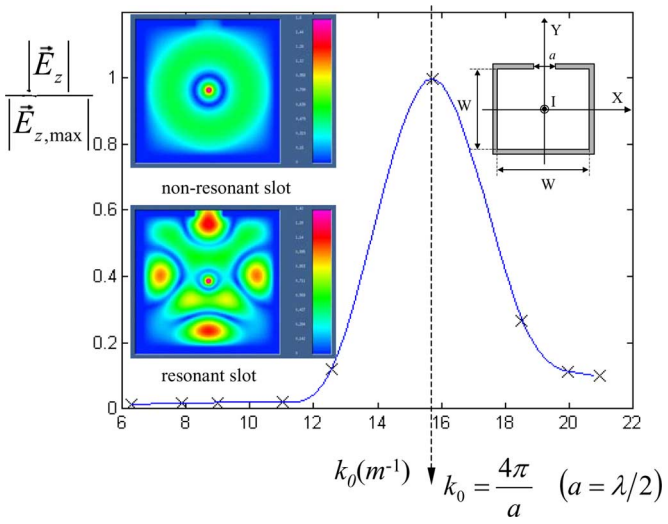


Fig. 10. Normalized radiated electric field interference produced by a linear current source line covered by a square slotted envelope and electric field patterns (in volts per meter) within the envelope for the resonant and nonresonant slot cases.

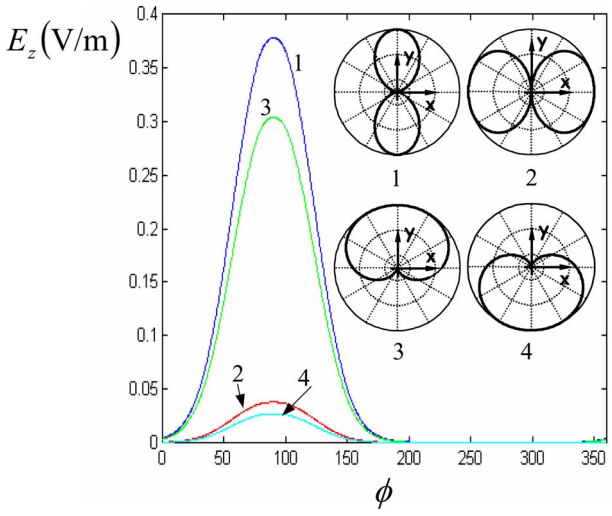


Fig. 11. Axial electric fields (in volts per meter) radiated by different current distributions and radiated perturbations and the corresponding unshielded normalized field patterns (in polar coordinates) for the different current distribution discussed in Section III-A.

a resonant slot. Numbers 1and 2 correspond to two current lines placed on the X-axis at $x = \pm\lambda/4$ with relative phases $(0°, 0°)$ and $(0°, 180°)$, respectively, whereas numbers 3 and 4 correspond to two current lines placed on the Y-axis at $y = \pm\lambda/8$ with relative phases $(0°, 90°)$ and $(0°, -90°)$, respectively. From the curves of radiated perturbation, it can be stated that no matter the unshielded radiation pattern, the shielded current perturbation is radiated in the direction of the slot ($\phi = 90°$). Nevertheless, it can also be observed that perturbation strength is strongly dependent on the unshielded perturbation pattern. When the free-space radiation points toward the slot (cases 1 and 3), there is a strong perturbation radiated by the slot but when the unshielded perturbation vanishes in the slot direction, the perturbation produced by the whole shielded system is significantly reduced

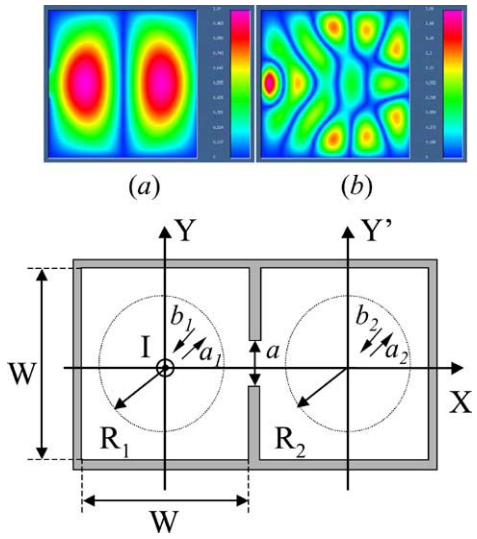


Fig. 12. Common mode intrasystem interference between two connected cavities of the same dimensions. The axial electric field (in volts per meter) in the victim cavity is plotted for (a) $Wk_0 = \pi\sqrt{5}/2$, and (b) resonant slot ($a = W\sqrt{2}/4,\ Wk_0 = 2\sqrt{2}\pi$).

(differences of near 20 dB can be observed in Fig. 11). It must be pointed out that the unshielded radiation patterns shown in Fig. 11 are far-field patterns, which can be easily measured in an anechoic chamber. Nevertheless, the shielded perturbation fields also plotted in Fig. 11 include the effect of the interaction of the near field produced by the linear current sources with the envelope; thus, the relationship between both the sets of field patterns is not so obvious as it seems to be in principle.

### C. Two Connected Cavity System

The intrasystem EMC problem consisting of two adjacent square cavities of the same dimensions ($W \times W$) and connected through a slot of length $a$ is analyzed throughout this section. Both common mode and differential mode currents are considered, along with empty and loaded victim cavities. The first intrasystem problem geometry is shown in Fig. 12: a 1-A interfering linear source current is placed in the center of the cavity on the left, and the electric field is computed in the empty cavity on the right (the victim cavity). The electric field coupled into the victim cavity depends on the interference frequency. When this frequency matches with one of the resonance frequencies of the equivalent 2-D closed resonant cavity, an interfering electric field with the corresponding resonant field pattern is coupled into this part of the enclosure. Otherwise, the coupling is almost negligible. However, not all possible resonant fields of the equivalent cavity are excited by the slot. For example, the axial electric field within the victim cavity is plotted in Fig. 12 for $Wk_0 = \pi\sqrt{5}/2$; although there are two degenerate modes sharing the same resonant frequency (the $TM_{21}$ and the $TM_{12}$), only one of them (the $TM_{21}$) is excited [field plot (a) in Fig. 12], because the other one vanishes along the plane $y = 0$, where the slot is placed. This behavior holds for all the resonant modes of the equivalent victim cavity. Additionally, the slot resonances also produce relevant interferences that are not

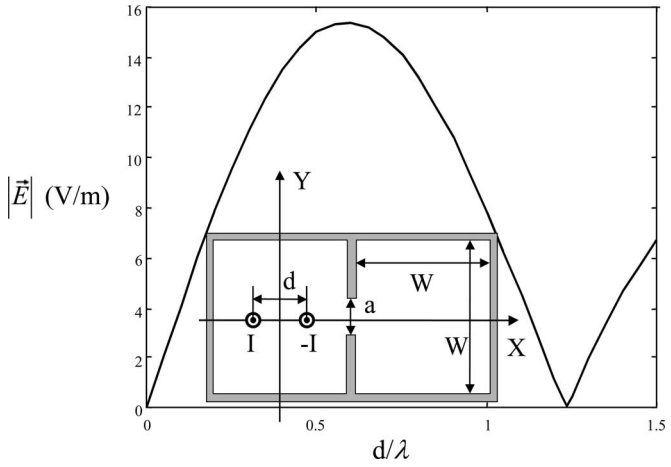


Fig. 13. Differential mode intrasystem interference analysis between two connected cavities of the same dimensions ($a = 0.2W$). The maximum axial electric field amplitude within the victim cavity for $Wk_0 = \pi\sqrt{5}/2$ is plotted versus the current line separation.

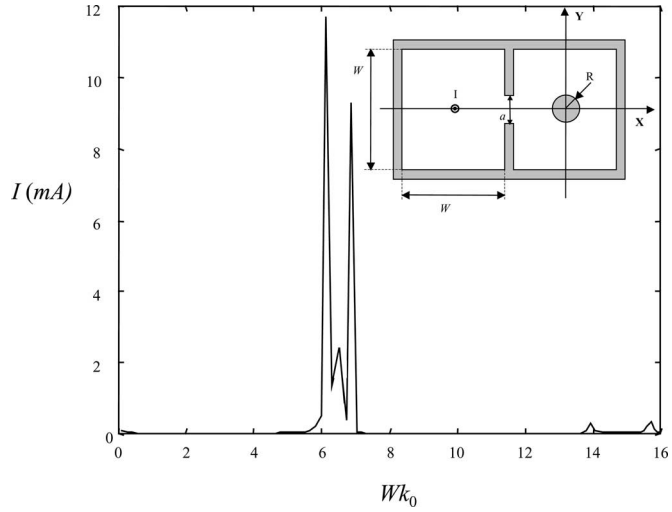


Fig. 14. Common-mode intrasystem interference analysis between two connected cavities of the same dimensions. The induced current in a perfectly conducting cylinder of radius $R = 0.1W$ placed in the center of the victim cavity is plotted versus the normalized wavenumber.

related at all with those produced due to the cavity resonances. Consider, for instance, the $TM_{22}$ mode of the victim cavity, that cannot be excited because its field pattern vanishes for $y = 0$ (the slot position); indeed, the electric field induced within the victim cavity for $Wk_0 = 2\sqrt{2}\pi$ (the $TM_{22}$ resonant wavenumber) through a nonresonant slot ($a = 0.2W$) drops more than 30 dB below the field coupled at the $TM_{21}$ resonant frequency. Nevertheless, if the slot length is modified in order to make it resonant ($a = W\sqrt{2}/4$), the electric field coupled within the victim cavity raises more than 30 dB with respect to the nonresonant case (thereby, producing an interference level equivalent to that produced by the $TM_{21}$ resonant mode).

The differential mode perturbation case is shown in Fig. 13. The same two connected square cavities system is considered, but now the interfering cavity on the left contains two 1-A linear current sources with opposite phases and separated by a distance $d$. The maximum electric field coupled into the victim cavity through a nonresonant slot ($a = 0.2W$) is plotted versus the separation $d$ for $Wk_0 = \pi\sqrt{2}$, which is the resonant frequency of the $TM_{11}$ mode of the equivalent 2-D square victim cavity (hence, the maximum interference field corresponds to the center of the cavity). If the effect of the shield was neglected and the interference sources were radiating in the free-space, the field along the X-axis would be maximum for $d = 0.5\lambda$, and it would vanish for $d = \lambda$. Thus, from the results shown in Fig. 13 and discussed earlier, the perturbation within the enclosure should be maximum for $d = 0.5\lambda$ and minimum for $d = \lambda$. However, the enclosure introduces some near-field effects, and the interference coupled into the victim cavity is maximum for $d = 0.6\lambda$ and it vanishes for $d = 1.2\lambda$.

Finally, the interference coupled into a nonempty enclosure is described in Fig. 14. In this case, the victim cavity on the right contains a centered perfectly conducting circular cylinder of radius $R = 0.1W$. The interference is produced by a 1-A linear current source parallel to the Z-axis in the center of the cavity on the left, and it is coupled to the victim cavity through a slot of length $a = 0.2W$, as shown in Fig. 14.

TABLE I
COMPARISON BETWEEN THE RESONANCE NORMALIZED WAVENUMBERS $Wk_r$, FOR THE FIRST $TM^z$ RESONANT MODES OF THE 2-D CAVITY ASSOCIATED TO THE VICTIM ENVELOPE OF THE STRUCTURE IN FIG. 8, AND THE NORMALIZED WAVENUMBERS OF THE CURRENT PEAKS INDUCED BY THE LINEAR CURRENT SOURCE $Wk_p$

| | | | | | | | |
|---|---|---|---|---|---|---|---|
| $Wk_r$ | 6.20 | 7.33 | 7.33 | 9.02 | 10.19 | 11.47 | 11.47 |
| $Wk_p$ | 6.12 | 6.42 | 6.87 | 13.97 | 15.70 | - | - |

The common-mode current perturbation induced on the cylinder is computed, and plotted in Fig. 14 versus the interfering current frequency. The graphic of the induced current presents several peaks that are somehow related with resonance phenomena. The resonant frequencies of the 2-D equivalent cavity problem associated to the victim part of the enclosure are listed in Table I, along with the frequencies corresponding to the current peaks in Fig. 14. The frequency at which the first current peak arises, $Wk_0 = 6.12$, and the resonant wavenumber of the first TM mode agree to within less than 1.3%. The electric field coupled into the victim cavity at this frequency, plotted in Fig. 15(a), also matches the first resonant TM-mode electric-field pattern. However, when the second TM mode coupling is explored, any significantly induced current is found on the cylinder surface at $Wk_0 = 7.33$, which is the corresponding resonant wavenumber, although the electric field perturbation within the cavity at this frequency indeed corresponds to the second TM-mode electric-field pattern, as shown in Fig. 15(b). Moreover, two additional peaks arise in the current graphic of Fig. 14 at $Wk_0 = 6.42$ and $Wk_0 = 6.87$. They are not associated to any resonant mode of the equivalent cavity. The origin of this apparently surprising result is found in the field symmetry. The second TM-mode field presents an even symmetric amplitude pattern but an odd phase distribution around the cylinder, thus, the electric current induced on part of the cylinder surface cancels out with the current induced on the other

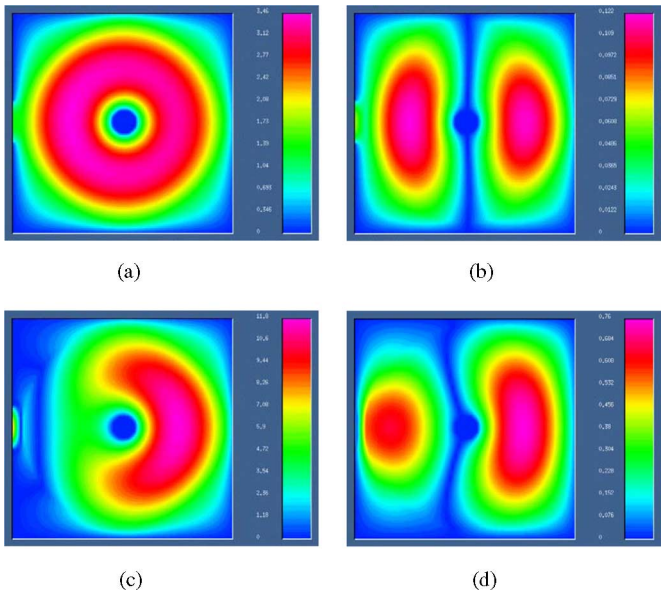


Fig. 15. Axial electric field induced in the victim cavity depicted in Fig. 14 for (a) $Wk_0 = 6.12$, (b) $Wk_0 = 7.33$, (c) $Wk_0 = 6.42$, and (d) $Wk_0 = 6.87$.

part, and the overall common current vanishes. However, both the amplitude and phase patterns of the first TM mode are even symmetric, and therefore, a nonvanishing common mode current is induced at the corresponding resonant frequency. On the other hand, the peaks at $Wk_0 = 6.42$ and $Wk_0 = 6.87$ appear due to some particular field distributions produced within the victim cavity, the so-called *banana modes* [13]. Banana modes are formed in this structure because the symmetry of the field pattern is lost due the effect of the slot, and a maximum appears on the opposite side, as shown in Fig. 15(c) and (d). These modes do not appear in the equivalent resonant cavity analysis because they are specifically produced by the effect of the slot equivalent reactance, which is removed when the resonant wavenumbers are computed. Since banana modes always present an unsymmetrical field pattern, nonvanishing common mode currents are associated to them. Banana modes are usually excited in loaded enclosures when the free space within the cavity is electrically small. Therefore, at frequencies $Wk_0 > 7$ only the highly symmetric TM modes are supported and the total common mode current induced on the cylinder surface vanishes. However, just below $Wk_0 = 14$, a TM mode with even symmetric amplitude and phase patterns is excited, producing a small peak in the current plot. Additionally, other nonvanishing induced current peaks appear whenever the field distribution is sufficiently unsymmetrical, like that at $Wk_0 = 15.7$ produced by the slot resonance. Anyway, the behavior of the banana modes is strongly dependent on geometric issues [14], and therefore, their effect must be assessed for any particular layout.

### *D. Effect of Finite Electrical Losses on the Envelope Resonances*

The discussions on the results of the previous examples clearly show that coupling phenomena are mainly due to resonances. These resonances severely affect the envelope performance, and can reduce its SE below 0 dB. The SE as low as $-20$ dB is reported in [3] for perfectly conducting boxes, and this means that the electric field amplitude within the envelope is ten times bigger than the field that would be if the shield were removed. This behavior can be explained as the effect of the constructive superposition of multiple reflections on the conducting walls at the resonant frequency.

TABLE II
COMPARISON BETWEEN THE SE PROVIDED BY AN EMPTY SLOTTED ENVELOPE WITH PERFECTLY CONDUCTING WALLS AND THAT OBTAINED FROM AN ENVELOPE WITH THE SAME DIMENSIONS BUT MADE OF A DIELECTRIC MATERIAL WITH $\varepsilon_r = 2.56$ AND $\sigma = 100$ S/m

| $Wk$ | mode | $SE\,(\sigma \to \infty)$ | $SE\,(\sigma = 100\ S/m)$ |
|---|---|---|---|
| $\pi$ | None | 30.0 dB | 24.0 dB |
| $\sqrt{2}\pi$ | $TM_{11}$ | -2.8 dB | 4.1 dB |
| $2\pi$ | None | 17.24 dB | 10.78 dB |
| $2\sqrt{2}\pi$ | $TM_{22}$ | 12.54 dB | 9.55 dB |

The resonant circuit quality factor $Q$ is the magnitude most widely used to represent the strength of a resonance. The envelope quality factor can be defined, in terms of stored energy and lost power, as $Q = 2\pi f_r U_T / W_L$, where $f_r$ is the resonant frequency, $U_T$ is the total energy (electric and magnetic) stored within the envelope, and $W_L$ is the overall lost power due to electric and magnetic losses. If the cavity walls are made of a lossy dielectric material, it can be expected that the $Q$ will diminish, and therefore, the effect of the resonance will be also weakened. A 2-D radiated susceptibility problem has been studied in order to explore the effects of reducing the walls conductivity. The envelope used in the simulation was as shown in Fig. 10, but now empty and with $0.05W$-width walls; a plane wave perturbation propagating along the Y-axis toward the origin was considered. The minimum SE was computed within the envelope using the definition of (18) at several frequencies, and the results are shown in Table II. At $Wk = \sqrt{2}\pi$ (the resonant frequency of $TM_{11}$ mode), the SE increases nearly by 7 dB when a shield made of a dielectric material with $\varepsilon_r = 2.56$ and $\sigma = 100$ S/m is used instead of a perfectly conducting one. At nonresonant frequencies (e.g., $Wk = \pi$ and $Wk = 2\pi$) there is still a high SE (the SE effectiveness reduction being comparable to the improvement achieved at the resonant frequency). Based on these results, the SE effectiveness of the box shown in Fig. 6 has been computed for frequencies ranging from 0 to 1.5 GHz using one commercial simulator based on the FEM (ANSYS). Fig. 16 shows the ANSYS solid model of the envelope along with the SE for a zero-width perfectly conducting box and for dielectric boxes of 4- and 2-mm-width walls made of a plastic with $\varepsilon = 2.56$ and $\sigma = 100$ S/m. In order to validate the FEM model, the SE computed for the perfectly conducting box is also compared with the experimental values reported in [3], showing a very good agreement. The metallic box has two resonant frequencies below 1.5 GHz ($f_r = 707.1$ MHz for the $TM_{110}$ and $f_r = 1.18$ GHz for the $TM_{210}$). As expected from the 2-D analysis, in both cases, the SE provided by the plastic envelope at the resonant frequencies is nearly 20 dB better than that obtained from the perfectly conducting one (no matter the wall width). Indeed, the SE of the plastic enclosure at frequencies above the

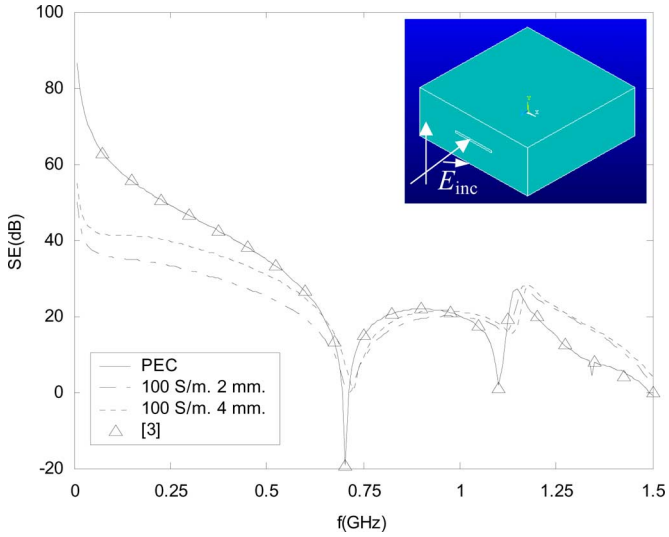


Fig. 16. SE of a slotted box for different materials. The shield dimensions are 30 cm × 30 cm × 12 cm; the slot dimensions are 10 cm × 0.5 cm, and it is placed on one of the narrow sides of the box.

first resonance is, in general, better than that of the conducting shield. At frequencies below the first resonance, although the SE obtained from the conducting screen is higher than that provided by the dielectric enclosure, the figures corresponding to the plastic box (SE > 40 dB for 4-mm-width walls) are still valid, depending on the specific application.

## IV. Conclusion

A hybrid GCA-FEM tool for 2-D electromagnetic analysis has been introduced, validated by comparing simulations and measurements, and then applied to different intersystem (radiated emission and susceptibility) and intrasystem (near field coupling) problems. As such, the examples considered in this work are simplified 2-D models of actual EMC problems; they provide a meaningful physical insight on several coupling and near-field phenomena produced within slotted enclosures that can hardly be studied using more realistic 3-D models due to the computational effort required to solve them. Although some acceleration techniques have been described in the recent literature, these improvements are being slowly incorporated into commercial simulators used by engineers dealing with EMC-oriented design. Practical EMC design is often based on the designer's experience, but 2-D simulation tools, like the GCA used in this paper, can help to roughly test design strategies or circuit layouts prior to apply them to more rigorous 3-D models. The design of a plastic enclosure presented here is a good example of how 2-D simulations can help to address a complex EMC problem: a set of fast (less than 24.4 s per frequency point on a COMPAQ DS20 single-processor workstation) simulations are performed in order to check the feasibility of the solution (the use of lossy dielectric enclosures improves SE at the resonant frequencies without a dramatic SE reduction at other frequencies), and to find a range of conductivities and wall widths that are then used in a time-consuming full-wave 3-D analysis oriented to assess the actual SE provided by a slotted plastic box (the average computation time in Fig. 16 was 490 s per frequency point also on a COMPAQ DS20 single-processor workstation).

In addition to the effect of losses on SE, the other results presented in this paper also show some physical phenomena that can arise within a slotted enclosure and that can produce EMC problems. Concerning the emission problem, slot resonances must be considered not only to reduce the radiated perturbations, but also to avoid intrasystem EMC problems, due to the strong field modification within the enclosure at the slot resonant frequency. Additionally, the radiation patterns of the noisy elements that are going to be shielded must be numerically or experimentally assessed before the slot emplacement is decided, since variations of nearly 20 dB can be found due to a wrong choice. These remarks are also valid for near-field intraystem problems, although in this case some results can slightly vary due to near-field effects. Near-field perturbations can also excite banana modes producing interferences at frequencies other than the resonant frequencies of the associated 2-D cavity, due to the effect of the slot equivalent circuit. Therefore, when banana modes were expected, the slot must be included into the model used to determine the frequencies where EMC problems are more likely. Additionally, it must be pointed out that not only SE values at single frequencies but also detailed field plots at potentially critical frequencies are needed in order to determine the best circuit layout within a slotted enclosure when dealing with actual EMC problems. Although all the examples shown in this work mainly involve squared envelopes, the proposed method can be extended to any rectangular enclosure just by increasing the number of ports (i.e., by using more cylinders). Obviously, the higher the number of ports, the higher the computation time needed to derive the scattering matrices, but this increment is still compensated by the fact that the scattering matrix is computed only once for a particular enclosure.

## References

[1] F. Olyslager *et al.*, "Numerical and experimental study of the shielding effectiveness of a metallic enclosure," *IEEE Trans. Electromagn. Compat.*, vol. 41, no. 3, pp. 202–213, Aug. 1999.

[2] Min Li *et al.*, "EMI from cavity modes of shielding enclosures-FDTD modeling and measurements," *IEEE Trans. Electromagn. Compat.*, vol. 42, no. 1, pp. 29–38, Feb. 2000.

[3] S. V. Georgakopoulos, C. R. Birtcher, and C. A. Balanis, "HIRF Penetration through apertures: FDTD versus measurements," *IEEE Trans. Electromagn. Compat.*, vol. 43, no. 3, pp. 283–294, Aug. 2001.

[4] J. V. Balbastre, L. Nuño, and M. Ferrando, "Susceptibility analysis or arbitrarily shaped 2-D slotted screens using a hybrid generalized scattering matrix-finite element method," *IEEE Trans. Electromagn. Compat.*, vol. 40, no. 1, pp. 47–54, Feb. 1998.

[5] C. A. Balanis, *Advanced Engineering Electromagnetics*. New York: Wiley, 1982.

[6] R. F. Harrington, *Time Harmonic Electromagetic Fields*. New York: McGraw-Hill, 1961.

[7] D. R. Wilton and R. Mittra, "A new approach to the calculation of electromagnetic scattering properties of two-dimensional bodies of arbitrary cross section," *IEEE Trans. Antennas Propagat.*, vol. 20, no. 3, pp. 310–317, May 1972.

[8] M. Abramowitz and I. A. Stegun, *Handbook of Mathematical Functions*. New York: Dover, 1970.

[9] J. M. Jin, *The Finite Element Method in Electromagnetics*. New York: Wiley, 1993.

[10] C. R. Paul, *Introduction to Electromagnetic Compatibility*. New York: Wiley, 1992.

[11] A. J. Lozano, A. Díaz, J. V. Balbastre, L. Nuño, A. B. Calvo, and J. Pitarch, "Damping resonances in a metallic enclosure through conductive polymers," in *Proc. 35th Eur. Microw. Conf.*, Oct. 2005, pp. 1399–1402.
[12] A. W. Rudge, K. Milne, A. D. Olver, and P. Knight, Eds., *The Handbook of Antenna Design Stevenage*. U.K: Peregrinus, 1982.
[13] R. W. Ziolkowski and J. B. Grant, "Scattering from cavity-backed apertures: The generalized dual series solution of the concentrically loaded E-pol slit cylinder problem," *IEEE Trans. Antennas Propagat.*, vol. AP-35, no. 5, pp. 504–528, May 1987.
[14] J. V. Balbastre, M. Bort, and L. Nuño, "Study of coupling phenomena in transmission line structures covered by slotted screens using the generalized circuital analysis,," in *Proc. 6th Top. Meet. Elect. Perform. Electron. Packag.*, San José, CA, 1997, pp. 157–160.

**Juan V. Balbastre** was born in Mislata, Spain, in August 1969. He received the Engineering and Ph.D. degrees from the Polytechnic University of Valencia, Valencia, Spain, in 1993 and 1996, respectively.

Since 1993, he has been a member of the research and teaching staff in the Department of Communications at the Polytechnic University of Valencia. In 2001, he joined the research staff of the ITACA Research Institute, Polytechnic University of Valencia. From 1998 to 2006, he was the Academic Vice-Dean at E.T.S.I. Telecomunicación of Valencia, Valencia. His current research interests include electromagnetic theory and computational electromagnetics applied to industrial microwave systems, electromagnetic compatibility, and radar.

**Luis Nuño** (M'95) was born in Valencia, Spain, in 1963. He received the Ingeniero (Ms.Eng.) degree from the Polytechnic University of Madrid (UPM), Madrid, Spain, and the Doctor Ingeniero (Ph.D.) degree from the Polytechnic University of Valencia (UPV), Valencia, in 1987 and 1993, respectively, both in telecommunication engineering.

He was with the Grupo de Radiación of the UPM in 1986–1988 and with the enterprise Ingeniería de Radiofrecuencias (IRSA) in 1988–1990. In 1990, he was a Teaching Assistant in the Department of Communications at UPV, where he became a Professor, in 2002. In April 2005, he became the Head of the EMC Laboratory (ICEM) R&D at UPV. His current research interests include numerical methods in electromagnetism, electromagnetic compatibility, and industrial applications of microwaves.

Prof. Nuño has been the Chairman of the International Electrotechnical Commission's subcommittee (IEC/SC 77B) on Electromagnetic Compatibility and High Frequency Phenomena since March 2006.

**Alejandro Díaz-Morcillo** (S'95–M'02) was born in Albacete, Spain, in 1971. He received the Ingeniero (Ms.Eng.) and Doctor Ingeniero (Ph.D.) degrees in telecommunication engineering, both from the Polytechnic University of Valencia (UPV), Valencia, Spain, in 1995 and 2000, respectively.

From 1996 to 1999, he was a Research Assistant in the Department of Communications at UPV. In 1999, he joined the Department of Information Technologies and Communications at the Polytechnic University of Cartagena (UPCT), Cartagena, Spain, as a Teaching Assistant, where he has been an Associate Professor since 2001. He leads the Electromagnetics and Matter Research Group at UPCT. His current research interests include numerical methods in electromagnetics, electromagnetic compatibility, and industrial microwave heating systems.

**Antonio Lozano** was born in El Verger, Spain. He received the Dipl.Ing. degree in telecommunications engineering from the Polytechnic University of Valencia (UPV), Valencia, Spain, in 2003. He is currently working toward the Ph.D. degree at the Polytechnic University of Cartagena (UPCT), Cartagena, Spain.

From 2003 to 2004, he was a Research Assistant with the Department of Communications, UPV. In 2004, he joined the Department of Information Technologies and Communications, UPCT, where he is currently an Associate Lecturer. His current research interests include electromagnetic compatibility and numerical techniques in electromagnetics.